# Application of the Steady-State Variable Nutation Angle Method for Faster Determinations of Long $T_1$s—An Approach Useful for the Design of Hyperpolarized MR Molecular Probes

Libertas Academica
FREEDOM TO RESEARCH

**Supplementary Issue: New Concepts in Magnetic Resonance as Applied to Cellular and In Vivo Applications**

Marc Jupin[1,*], Ayelet Gamliel[1,*], Yonatan Hovav[2], Jacob Sosna[1], J. Moshe Gomori[1] and Rachel Katz-Brull[1]

[1]Department of Radiology, Hadassah-Hebrew University Medical Center, Jerusalem, Israel. [2]Weizmann Institute of Science, Rehovot, Israel.
*These authors contributed equally to this article.

**ABSTRACT:** In the dissolution-dynamic nuclear polarization technique, molecular probes with long $T_1$s are preferred. $^{13}C$ nuclei of small molecules with no directly bonded protons or $sp^3$ $^{13}C$ nuclei with proton positions substituted by deuterons may fulfill this requirement. The $T_1$ determination of such new molecular probes is crucial for the success of the hyperpolarized observation. Although the inversion-recovery approach remained by and large the standard for $T_1$ measurements, we show here that the steady-state variable nutation angle approach is faster and may be better suited for the determination of relatively long $T_1$s in thermal equilibrium. Specifically, the $T_1$ of a new molecular probe, [uniformly labeled (UL)-$^{13}C_6$, UL-$^{2}H_8$]2-deoxy-D-glucose, is determined here and compared to that of [UL-$^{13}C_6$, UL-$^{2}H_7$]D-glucose.

**KEYWORDS:** $T_1$ measurement, steady state, variable nutation angle, DNP probes

**SUPPLEMENT:** New Concepts in Magnetic Resonance as Applied to Cellular and In Vivo Applications

**CITATION:** Jupin et al. Application of the Steady-State Variable Nutation Angle Method for Faster Determinations of Long $T_1$s—An Approach Useful for the Design of Hyperpolarized MR Molecular Probes. *Magnetic Resonance Insights* 2015:8(S1) 41–47 doi:10.4137/MRI.S29358.

**TYPE:** Original Research

**RECEIVED:** May 6, 2015. **RESUBMITTED:** July 16, 2015. **ACCEPTED FOR PUBLICATION:** July 26, 2015.

**ACADEMIC EDITOR:** Sendhil Velan, Editor in Chief

**PEER REVIEW:** Five peer reviewers contributed to the peer review report. Reviewers' reports totaled 1,232 words, excluding any confidential comments to the academic editor.

**FUNDING:** This study was supported by an ISF grant (No. 284/10) and an ERC grant (No. 338040) to RK-B. The authors confirm that the funder had no influence over the study design, content of the article, or selection of this journal.

**COMPETING INTERESTS:** Authors disclose no potential conflicts of interest.

**COPYRIGHT:** © the authors, publisher and licensee Libertas Academica Limited. This is an open-access article distributed under the terms of the Creative Commons CC-BY-NC 3.0 License.

**CORRESPONDENCE:** rkb@hadassah.org.il

Paper subject to independent expert blind peer review. All editorial decisions made by independent academic editor. Upon submission manuscript was subject to anti-plagiarism scanning. Prior to publication all authors have given signed confirmation of agreement to article publication and compliance with all applicable ethical and legal requirements, including the accuracy of author and contributor information, disclosure of competing interests and funding sources, compliance with ethical requirements relating to human and animal study participants, and compliance with any copyright requirements of third parties. This journal is a member of the Committee on Publication Ethics (COPE).

Published by Libertas Academica. Learn more about this journal.

## Introduction

The dissolution-dynamic nuclear polarization (DNP) technique has revolutionized the solution state and in vivo nuclear magnetic resonance (NMR) spectroscopy field, by offering an increase of >10,000-fold in signal.[1] However, this approach is limited by the need to obtain a substrate molecule that has a reporting nucleus with long $T_1$. This is because it takes a minimum of 20 seconds for the processes of dissolution and transfer of the hyperpolarized liquid samples to an NMR scanner. During this time and further on, the induced massive spin polarization decays at a rate that is governed by the spin–lattice relaxation with a time constant $T_1$. Therefore, useful molecular probes for this technique need to have nuclei with slow relaxation rates, ie, $5T_1 > 20$ seconds.

$^{13}C$ of small molecules that have no direct protons attached, eg, carbonyl, carboxyl, certain quaternary carbons, or perdeuterated carbons,[2] may fulfill this requirement. Other requirements for successful dissolution-DNP molecular probes relate to their biological activity.[3,4] Molecular probes for this technique should be transported and metabolized within very few minutes to enable the evaluation of their activity, while the hyperpolarized signal is still at a sufficient level.[5] The selection of a metabolite candidate for development into a dissolution-DNP molecular probe depends heavily on the $T_1$ of the reporting nuclei in this probe and on the determination of this $T_1$.

$T_1$ can in principle be determined based on the decay curve of the hyperpolarized signal.[6] This is an extremely fast and reliable way of measuring $T_1$,[4,6] provided that the effects of radio-frequency (RF) pulses and the temperature are well controlled during the measurement. However, this technique critically depends on the availability of a dissolution-DNP polarizer, which is much less abundant than NMR spectrometers or magnetic resonance imaging (MRI) scanners. Also, it is preferred that a $^{13}C$ (or $^{13}C$ and D)-labeled compound is available. Non-$^{13}C$-labeled compounds have a 100-fold lower signal, which could be a limiting factor, as hyperpolarized spectra cannot benefit from the advantages of signal averaging as thermal equilibrium measurements can. Because the measurement of $T_1$ is done as part of the design of a new molecular

probe and as an initial step to avoid costly nonuseful custom synthesis efforts, this is a true limitation in the design of novel molecular probes for the dissolution-DNP technology.

The inversion-recovery (IR) technique is by and large the sole $T_1$ determination approach in use today in solutions. This technique depends on the time required to reach thermal equilibrium, ie, durations longer than $5T_1$, which results in very long measurement times for nuclei that have a long $T_1$ and are low in abundance or concentration (due to the high number of scans required for satisfactory signal-to-noise ratios). In 1971, Christensen et al[7] introduced the steady-state variable nutation angle (SSVN) method, which enables fast $T_1$ measurements. This method was revisited by Gupta[8] in 1977 and by Homer and Beevers[9] in 1985. The latter two studies described the potential and limits of the SSVN method for $T_1$ determinations. The method requires dummy scans to reach steady states and pulse repetition times (TR) that are longer than $T_2$* and can be shorter or longer than $T_1$. The useful range for TR is dependent on the actual $T_1$ and on the number of dummy scans applied.[8,9] Altogether, the SSVN approach was shown to result in $T_1$ measurements that could be 100 times faster than the traditional IR method.[9]

These investigations of the SSVN approach, as well as the earlier works of Look and Locker,[10] served as the basis for the development of the saturation-recovery technique for $T_1$ estimations (multiple 90° RF pulses at relatively short repetition times) as well as for steady-state imaging.[11] Despite this large body of work, validation, and tremendous implications for MRI, by and large, the SSVN approach had not been used for $T_1$ determinations in solution-state NMR. Here we test the utility of the linear regression version of the SSVN approach (Equ. 3, below)[8,9] for $T_1$ determination of specific probes. This is part of a characterization effort of stable-isotope-labeled sugar molecular probes that are being evaluated for use in dissolution-DNP hyperpolarized magnetic resonance (MR).

Glucose is the most important and predominant sugar in life and is metabolized by prokaryotes and eukaryotes. It is the starting material for multiple biochemical pathways, eg, glycolysis, glycogenesis, streptomycin biosynthesis, and starch and sucrose metabolism. In vivo and in vitro MR studies (MRs) following the metabolic fate of $^{13}$C-labeled glucose[12] have contributed to the understanding of brain,[13–17] liver,[18] and muscle[19,20] metabolism in mammals as well as the formation of gallic acid in plants and fungi.[21] [Uniformly labeled (UL)-$^{13}C_6$, UL-$^{2}H_7$]D-glucose is a relatively new molecular probe for dissolution-DNP that was found useful for hyperpolarized glucose MRI[22] and hyperpolarized MR monitoring of glucose metabolism in tumors,[23] yeast,[24] and enzymatic reactions.[25] The nonmetabolic derivative of glucose, $^{18}$F-deoxyglucose, has been used in nuclear medicine for diagnosing and staging diseases for more than 20 years. Nonradioactive 2-deoxy-D-glucose has been used to study erythrocytes[26] and brain[27,28] metabolism. The radioactive analog [$^{14}C_1$]2-deoxy-D-glucose was also used in the MR study of brain metabolism.[29]

In an attempt to follow the footsteps of this highly valuable molecular probe and produce a nonradioactive analog that could be useful for hyperpolarized MRI, the [UL-$^{13}C_6$, UL-$^{2}H_8$]2-deoxy-D-glucose analog was designed and synthesized. Here we determine the $T_1$ of position 1 of the α and β anomers of this novel probe using the linear regression version of the SSVN method. The results are validated with respect to an IR measurement of the same sample and compared to the respective $T_1$s of the [UL-$^{13}C_6$, UL-$^{2}H_7$] D-glucose probe. Using these specific molecules and anomers we determined the effect of substituting a hydroxyl group (in [UL-$^{13}C_6$, UL-$^{2}H_7$]D-glucose) with a deuterium atom (in [UL-$^{13}C_6$, UL-$^{2}H_8$]2-deoxy-D-glucose) on an sp3 $^{13}$C spin-lattice relaxation.

## Materials and Methods

**Materials.** [UL-$^{13}C_6$, UL-$^{2}H_7$]D-glucose (99% $^{13}$C, 97–98% $^{2}$H) was obtained from Cambridge Isotope Laboratories. [UL-$^{13}C_6$, UL-$^{2}H_8$]2-deoxy-D-glucose (99% $^{13}$C, 99% $^{2}$H) was obtained from 13C Molecular.

**NMR samples.** The [UL-$^{13}C_6$, UL-$^{2}H_7$]D-glucose and [UL-$^{13}C_6$, UL-$^{2}H_8$]2-deoxy-D-glucose concentration in the NMR samples was 400 mM in 10:90% $D_2O$:$H_2O$.

**NMR measurements.** Samples were placed in 5 mm tubes and measured at 11.8 T (Bruker) with a 5-mm PABBO probe. Temperature was calibrated to 37°C, and data were recorded using the standard IR (RD–180°–$\tau$–90°–AD) pulse sequence and the SSVN (RD–$\theta$–AD) pulse sequence, where RD is the recovery delay (seconds); $\tau$ is the time increment (seconds); AD is the time of acquisition (seconds); and $\theta$ is the RF pulse nutation angle. For the latter pulse sequence, data were recorded after five dummy scans to ensure that a steady state was formed. To eliminate residual signals, we used phase cycling ($x$, $-x$, $-x$, $x$, $y$, $-y$, $-y$, $y$).

The 90° pulses were calibrated by determining the 360° pulse widths for each sample and each measurement. For the SSVN measurement, the $\theta$ pulse duration was increased from one to nine microseconds, with one microsecond steps. One microsecond corresponded to an 8.6° nutation angle. Thus, $\theta$ varied over 8.6–77.4°. These SSVN $\theta$ values were chosen according to the work of Christensen et al[7] who showed that with four to five dummy scans, the optimal angles for $T_1$ determination were <90°.

**Spectral processing.** All spectra were processed using Mnova (Mestrelab Research). The $^{13}$C resonances of the α and β anomers of the deuterated and the protonated (isotopic impurity) nuclei were identified based on previous literature for D-glucose[30–33] and D-deoxyglucose[34,35] and using the simulation of the multiplet signals. For convenience, the chemical shift of both the glucose and the deoxyglucose spectra was calibrated using the deuterated α-glucose and α-deoxyglucose $C_1$ signals at 92.77 ppm.

Integrated signal intensities were used in the analyses of the time or nutation angle-dependent signal behavior.

The integral regions that were used for the analyses of the deuterated α- and β-glucose $C_1$s were 92.85–93.41 ppm and 96.60–97.18 ppm, respectively. For the analyses of the deuterated α- and β-deoxyglucose $C_1$s, the integral regions that were used were 92.87–93.41 ppm and 94.91–95.44 ppm, respectively.

The spectra of both the [UL-$^{13}C_6$, UL-$^2H_8$]2-deoxy-D-glucose and the [UL-$^{13}C_6$, UL-$^2H_7$]D-glucose compounds and their anomer structures are shown in Figure 1. The rational for selecting the integration regions described above is as follows. Because the measurements were recorded without decoupling of the proton or the deuterium interaction, the $^{13}C$ signals of both the labeled molecules and the protonated isotopic impurity molecules appear split. Simulating these spin systems (Fig. 2) showed that the $^{13}C$ resonances of the isotopic impurity and the labeled compound overlap. The region of overlap is shown in Figure 2, on the right-hand side of the major multiplet. For the analyses of $T_1$, in order to avoid a possible effect of this overlap, we used an integration region consisting of the two most left-hand side peaks of the major multiplets, which were farthest from the overlapping isotopic impurity signals.

**$T_1$ analyses.** The time or the nutation angle-dependent signal behavior in the IR and the SSVN experiments can be described, respectively, by

$$M_\tau = M_0\left\{1-2\exp\left(-\tau / T_1\right)\right\} \quad (1)$$

and

$$M_\theta = \frac{\left\{M_0\left(1-\exp\left(\frac{-\mathrm{TR}}{T_1}\right)\right)\sin\theta\right\}}{\left\{1-\exp\left(\frac{-\mathrm{TR}}{T_1}\right)\cos\theta\right\}} \quad (2)$$

where $M_0$ and $M_\tau$ are the magnetization vectors at thermal equilibrium and following an inter-pulse delay $\tau$, respectively, and TR is the repetition time, TR = RD + AD.[8]

$T_1$ was extracted from experiments with a variable nutation angle and a given TR time. For this, it is convenient to rewrite Equ. 2 as Equ. 3, which can be analyzed by a linear fit for a fixed TR value, considering $M_\theta/\sin\theta$ vs. $M_\theta/\tan\theta$ (Equ. 3)[8]:

$$\frac{M_\theta}{\sin\theta} = \left(\frac{M_\theta}{\tan\theta}\right)\exp\left(\frac{-\mathrm{TR}}{T_1}\right) + M_0\left(1-\exp\left(\frac{-\mathrm{TR}}{T_1}\right)\right) \quad (3)$$

This approach is the linear regression version of the SSVN method. $T_1$ is then extracted from the slope of the resulting line and $M_0$ from the intercept at $(M_\theta/\tan\theta) = 0$. In principle, it is also possible to carry out the measurement with a variable TR and a fixed nutation angle. The saturation-recovery technique is a variant of this steady-state approach where the fixed angle is set at 90° and TR is varied. We chose the former option (fixed TR) in order

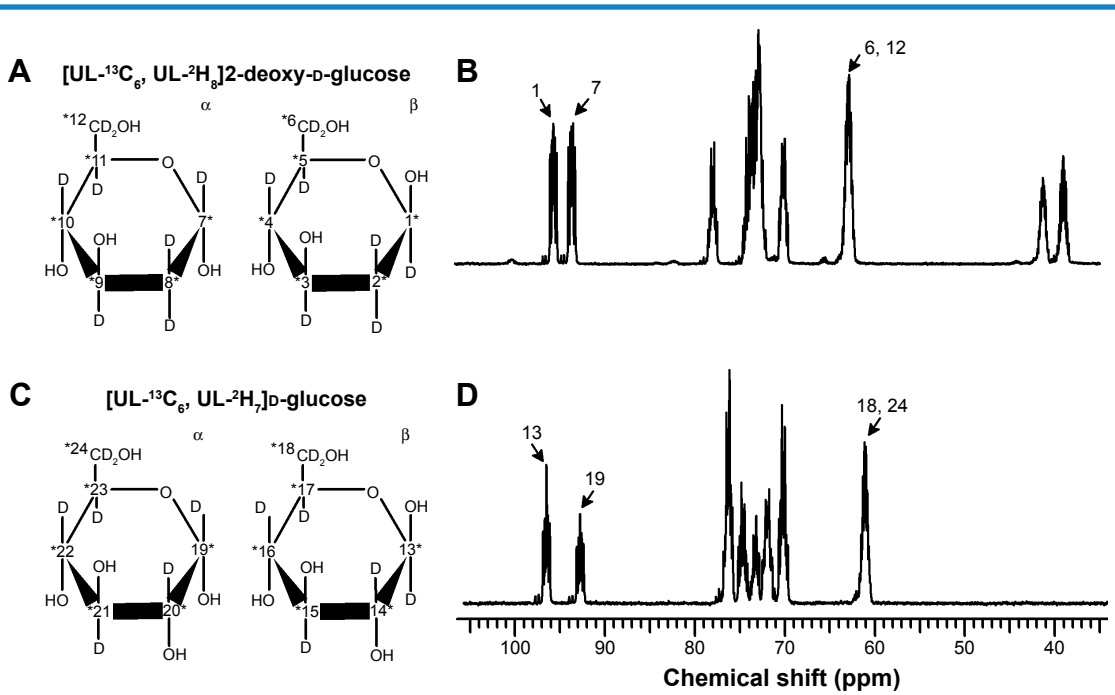


**Figure 1.** $^{13}C$ spectra and structures of [UL-$^{13}C_6$, UL-$^2H_8$]2-deoxy-D-glucose and [UL-$^{13}C_6$, UL-$^2H_7$]D-glucose: (**A**) the chemical structures of the α and β anomers of [UL-$^{13}C_6$, UL-$^2H_8$]2-deoxy-D-glucose, (**B**) a $^{13}C$ spectrum of [UL-$^{13}C_6$, UL-$^2H_8$]2-deoxy-D-glucose, showing the signals of the α and β anomers, (**C**) the chemical structures of the α and β anomers of [UL-$^{13}C_6$, UL-$^2H_7$]D-glucose, and (**D**) a $^{13}C$ spectrum of [UL-$^{13}C_6$, UL-$^2H_7$]D-glucose, showing the signals of the α and β anomers. The marked signals were assigned according to previous reports.[19–22]

**Notes:** *Indicates labeled $^{13}C$. D indicates deuterium ($^2H$). The various $^{13}C$ positions in both anomers are marked by numerals in the structures for convenience of reference.

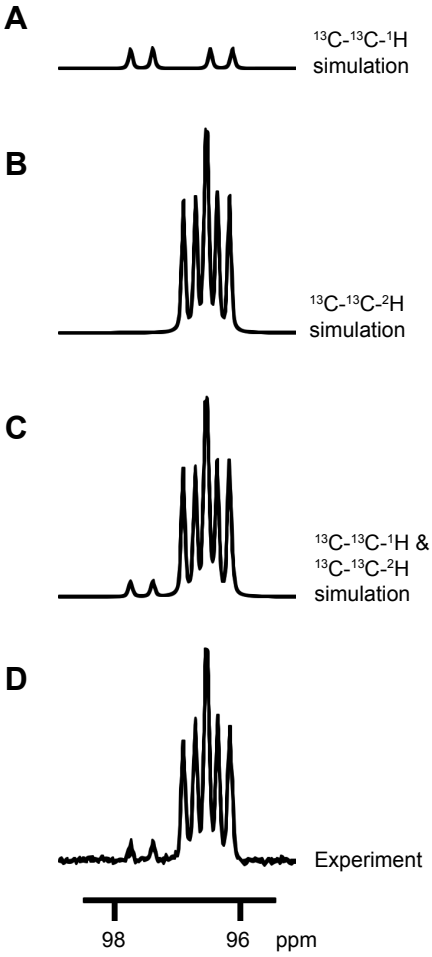


**Figure 2.** The simulations of the β-[UL-$^{13}C_6$, UL-$^{2}H_7$]D-glucose $^{13}C_1$ signals in the fully labeled compound and in an isotopic impurity (**A**–**C**) in comparison to the experimental spectrum (**D**). (**A**) The signal of the $^{13}C_1$ that is bonded to proton (isotopic impurity) is split due to the interaction with $^{13}C_2$, $^{13}C_3$, $^{13}C_5$, and the proton nucleus directly bonded to it. The J-coupling constants used in this simulation were as follows: $J_{C1-C2}$ = 45 Hz, $J_{C1-C3}$ = 4 Hz, $J_{C1-C5}$ = 4 Hz, and $J_{C1-H}$ = 161 Hz, based on a previous characterization.[17] (**B**) The signal of the $^{13}C_1$ of the deuterium-labeled compound β-[UL-$^{13}C_6$, UL-$^{2}H_7$]D-glucose is split due to the interaction with $^{13}C_2$, $^{13}C_3$, and $^{13}C_5$ and the deuterium nucleus directly bonded to it. The J-coupling constants used in this simulation based on a previous characterization were as follows[17]: $J_{C1-C2}$ = 44 Hz, $J_{C1-C3}$ = 3.5 Hz, $J_{C1-C5}$ = 4 Hz, and $J_{C1-D}$ = 24.5 Hz. (**C**) The signal resulting from a combination of the upper and middle panels. (**D**) The experimental signal of $C_1$ of β-[UL-$^{13}C_6$, UL-$^{2}H_7$]D-glucose that also contains the isotopic impurity of a protonated $C_1$ (or β-[UL-$^{13}C_6$, 2,3,4,5,6,6-$^{2}H_6$]D-glucose). The experimental spectrum matches the simulated spectra extremely closely; it is presented separately for the purpose of discerning the two. The signals of $^{13}C_1$ of the α anomer showed the same split pattern. The signals of $^{13}C_1$ of the α and β anomers of [UL-$^{13}C_6$, UL-$^{2}H_8$]2-deoxy-D-glucose showed a similar split pattern, although prior J-coupling constants for this molecule are not available in the literature as this molecule is first introduced here, to the best of our knowledge.

to keep the TR as short as possible for the benefit of time efficiency.

According to the previous analysis of the linear regression version of the SSVN method,[8] it was shown that optimal fits were obtained at pulse angles ≤90°[7,9] and TRs in the range of 0.1–10$T_1$. Previously, the $T_1$ of [UL-$^{13}C_6$, UL-$^{2}H_7$] D-glucose was estimated at 12 seconds.[22] We used TRs of 7 and 14 seconds corresponding to estimated 0.6$T_1$ and 1.2$T_1$, respectively. The same TR values were used for [UL-$^{13}C_6$, UL-$^{2}H_8$]2-deoxy-D-glucose.

Curve and linear fittings for analyses of IR and SSVN data, respectively, were performed using nonlinear least squares and linear least squares carried out in MATLAB (MathWorks, Inc.). The 95% confidence interval was determined using MATLAB's confint function.

## Results

A typical data set for the SSVN method for the $C_1$ position in the [UL-$^{13}C_6$, UL-$^{2}H_8$]2-deoxy-D-glucose sample is shown in Figure 3A. The nutation angle, $\theta$, was varied over ~9–77°, while the TR was fixed at 7 or 14 seconds. These TR values were selected based on our previous work with [UL-$^{13}C_6$, UL-$^{2}H_7$]D-glucose at the same magnetic field[22] (see Materials and methods). Nevertheless, we note that the determination of $T_1$ is the aim of the experiment and it is not necessarily known or approximated beforehand. Without a prior estimate of $T_1$, it is likely that at least two measurements at two different TRs can provide increased confidence that the $T_1$ is indeed determined with a suitable TR.

Figure 3B shows the data that were obtained for the β anomer, plotted as $M_\theta$/sin $\theta$ vs. $M_\theta$/tan $\theta$, to enable analysis by a linear fit to Equ. 3. $T_1$ was determined from the slope of this line. $M_0$ could be obtained from the $y$-axis intercept, but it was not needed here.

The same analysis was also carried out for the α anomer of [UL-$^{13}C_6$, UL-$^{2}H_8$]2-deoxy-D-glucose as well as for the α and β anomers of [UL-$^{13}C_6$, UL-$^{2}H_7$]D-glucose. The results are summarized in Table 1.

Considering the confidence intervals of the $T_1$ values in Table 1, it can be said that the values obtained using the SSVN method with TR 7 or 14 seconds are similar. These values are also similar to the values obtained by the IR method. The $T_1$ values obtained for the $C_1$ position of both α and β anomers of both molecules appear the same considering the confidence intervals of all values. The $T_1$s of other positions were not determined here due to the complexity to identify some of the positions and the heavy overlap between positions due to the complex $^{13}C$ and deuterium split of all positions. Nevertheless, we believe that for the purpose of demonstrating the utility of the SSVN approach, the investigation of the same position ($C_1$), in both compounds and both anomers of each compound, was sufficient.

## Discussion

We showed that the linear regression version of the SSVN method for $T_1$ determination of nuclei with slow spin–lattice relaxation provides similar results as the standard IR method, with the advantage of being faster. Using SSVN method, with a TR of 14 seconds (about 0.8–1.4$T_1$, according to the

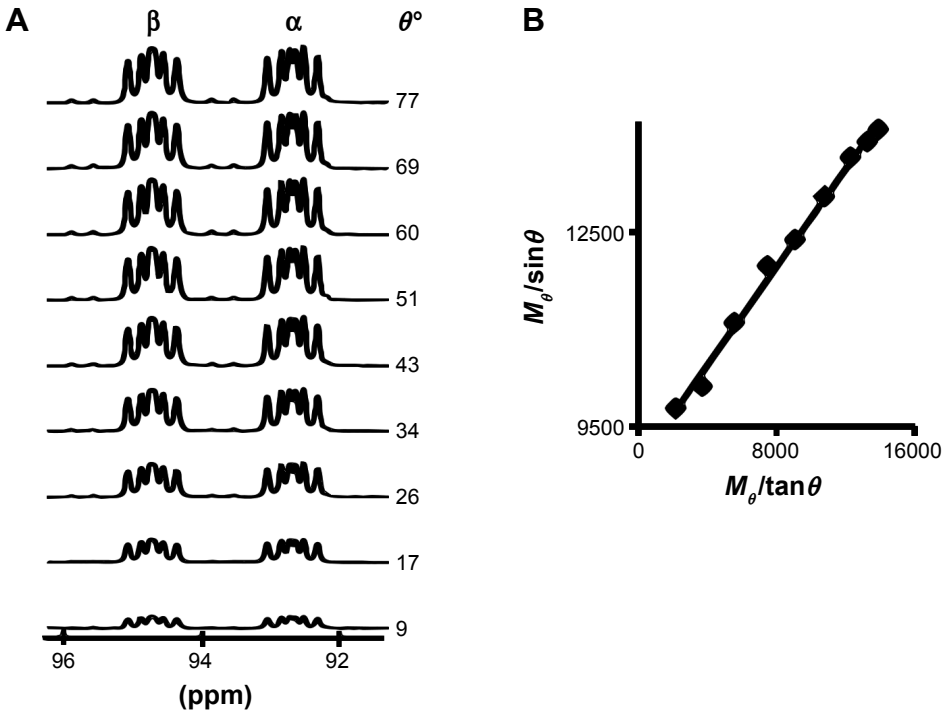


**Figure 3.** (**A**) A typical SSVN data set showing the signals of $^{13}C_1$ of α- and β-[UL-$^{13}C_6$, UL-$^{2}H_8$]2-deoxy-D-glucose at variable nutation angles ($\theta$) acquired with a TR of 14 seconds, 20 repetitions, and five dummy scans. The pulse duration was incremented from one to nine microseconds, with one microsecond steps. One microsecond corresponded to a 8.6° nutation angle. Thus, $\theta$ was varied over 8.6–77.4°. (**B**) A fit of the SSVN data shown in (**A**) for the β anomer using Equ. 3. The resulting linear fit was $M_\theta/\sin\theta = (M_\theta/\tan\theta)\ 0.377 + 8946$ with an $R^2$ of 0.99. According to Equ. 3, the slope (0.377) equals to exp (–TR/$T_1$). Thus, here the $T_1$ value is calculated from the slope for a known TR of 14 seconds to be 14.4 seconds.

confidence intervals) and recording 20 scans (preceded by 5 dummy scans) with nine iterations, the total scan time was 52.5 minutes, whereas using IR with seven time increments, the total scan time was 1.5 hours. If the perfectly matching IR experiment would have been performed, ie, with the last time increment at least three times $T_1$, and nine time increments were applied as in the SSVN method, all with a TR $\geq 5T_1$, the scan time would be about four hours. This has a huge impact on the time spent for testing and evaluating the various potential metabolites and the possible $^{13}C/^{2}H/^{15}N$ labeling for DNP–NMR metabolic studies.[3] Considering $T_1$ measurements of low solubility materials or compounds at natural abundance that could take several days using the IR method, it renders the SSVN method a crucial enabling methodology.

In addition to the direct acquisition time calculation, another factor that is in favor of the SSVN approach, as it is applied here, is that all the data points have a significant and measureable signal. However, in the IR approach, data points that are crucial for the accuracy of the curve fitting, ie, data points that are in the middle of the curve and close to $\tau_0$, are those with an inherently low signal. In a long IR experiment, one may find that several hours or a day had been spent on acquiring a data point that shows minimal to zero signal. This leads to data sets that are noisier and have loss of precision in the results, which may be also manifested as the wider confidence intervals. Although not the aim of the current study, such an analysis of the effect of noisier data can be performed as well, as previously shown by Chang et al in 2008.[36]

**Table 1.** $T_1$ values calculated using the SSVN method and compared to the IR method.

| COMPOUND AND ANOMER—POSITION $C_1$ | INTEGRAL REGION (PPM) | $T_1$ (s) | | |
|---|---|---|---|---|
| | | IR* | SSVN* TR = 7 s | SSVN* TR = 14 s |
| α-[UL-$^{13}C_6$, UL-$^{2}H_7$]D-glucose | 92.85–93.41 | **12.7** (10.2, 17.0) | **11.7** (9.8, 14.3) | **12.7** (12.3, 13.2) |
| β-[UL-$^{13}C_6$, UL-$^{2}H_7$]D-glucose | 96.60–97.18 | **14.1** (11.9, 17.3) | **12.2** (10.6, 14.1) | **13.0** (12.7, 13.4) |
| α-[UL-$^{13}C_6$, UL-$^{2}H_8$]2-deoxy-D-glucose | 92.87–93.41 | **14.9** (13.7, 16.3) | **14.0** (13.6, 14.4) | **13.9** (13.0, 14.9) |
| β-[UL-$^{13}C_6$, UL-$^{2}H_8$]2-deoxy-D-glucose | 94.91–95.44 | **14.6** (13.5, 15.9) | **13.9** (13.3, 14.5) | **14.4** (13.4, 15.4) |

**Note:** *The $T_1$ values are given with the 95% confidence interval written in brackets.

One caveat to the SSVN approach is the need to calibrate carefully the nutation angle. Although errors in the 90° and 180° pulses will lead to imperfect experiments and loss of accuracy of the IR results, the results of the SSVN approach appear much more sensitive to such errors due to the direct use of the nutation angle value as a factor in the calculation of $T_1$. Nevertheless, we note that while errors in flip angle determination in the IR experiments can be very complex to correct for, a retrospective correction in the flip angle value for the SSVN experiment can be implemented easily.

In the current study, decoupling of protons or deuterons was not used as this is known to reduce the apparent relaxation time due to magnetization transfer from the attached nuclei, hence leading to a measured $T_1$ value that is shorter than the true relaxation time.[6] For this reason, the J-couplings due to the $^{13}C$-$^{1}H$ and $^{13}C$-$^{2}H$ interactions are visible. The split pattern was fully simulated for the $C_1$ signal of β-[UL-$^{13}C_6$, UL-$^{2}H_7$] D-glucose (Fig. 2) and aided in determining the required integral regions for analysis. Simulation was performed only for the [UL-$^{13}C_6$, UL-$^{2}H_7$]D-glucose molecule because prior knowledge on the J-coupling constants in this case was available. Nevertheless, we note that this split pattern was similar in both compounds and both anomers.

Finally, the $T_1$ of the $C_1$ position does not seem to be affected by the change in its neighboring group from a hydroxyl moiety to a deuteron (in [UL-$^{13}C_6$, UL-$^{2}H_7$] D-glucose and [UL-$^{13}C_6$, UL-$^{2}H_8$]2-deoxy-D-glucose). Further studies are required to fully assign the split signals of [UL-$^{13}C_6$, UL-$^{2}H_8$]2-deoxy-D-glucose and attempt the estimation of the $T_1$ of further positions in this molecule. We note that the $^{13}C$ positions with signals that are heavily overlapping with the signals of other positions may not be amenable for $T_1$ analysis. Here we focused on the signals of position 1 as these were distinct.

## Conclusion

Because the hyperpolarized MR technology requires molecular probes with long $T_1$, methods for $T_1$ determination that are reliable and time effective are needed. We found that the SSVN method provides this solution. It saves a significant amount of time and generates results that are similar to the standard IR method. It is demonstrated here that for an sp3 $^{13}C$ nucleus, the substitution of a directly bonded hydroxyl group with a deuteron does not affect $T_1$.

## Acknowledgments

We thank Shimon Vega for useful discussions.

## Author Contributions

Conceived and designed the experiments: MJ, AG, RKB. Analyzed the data: MJ, AG. Wrote the first draft of the manuscript: MJ, AG, RKB. Contributed to the writing of the manuscript: MJ, AG, YH, RKB. Agree with manuscript results and conclusions: MJ, AG, YH, JS, JMG, RKB. Jointly developed the structure and arguments for the paper: MJ, AG, YH, JS, JMG, RKB. Made critical revisions and approved final version: MJ, AG, YH, JS, JMG, RKB. All authors reviewed and approved of the final manuscript.

## REFERENCES

1. Ardenkjaer-Larsen JH, Fridlund B, Gram A, et al. Increase in signal-to-noise ratio of >10,000 times in liquid-state NMR. *Proc Natl Acad Sci U S A*. 2003;100(18):10158–10163.
2. Allouche-Arnon H, Lerche MH, Karlsson M, Lenkinski RE, Katz-Brull R. Deuteration of a molecular probe for DNP hyperpolarization—a new approach and validation for choline chloride. *Contrast Media Mol I*. 2011;6(6):499–506.
3. Kurhanewicz J, Vigneron DB, Brindle K, et al. Analysis of cancer metabolism by imaging hyperpolarized nuclei: prospects for translation to clinical research. *Neoplasia*. 2011;13(2):81–97.
4. Meier S, Jensen PR, Karlsson M, Lerche MH. Hyperpolarized NMR probes for biological assays. *Sensors (Basel)*. 2014;14(1):1576–1597.
5. Harada M, Kubo H, Abe T, Maezawa H, Otsuka H. Selection of endogenous $^{13}C$ substrates for observation of intracellular metabolism using the dynamic nuclear polarization technique. *Jpn J Radiol*. 2010;28(2):173–179.
6. Day IJ, Mitchell JC, Snowden MJ, Davis AL. Applications of DNP-NMR for the measurement of heteronuclear $T_1$ relaxation times. *J Magn Reson*. 2007;187(2):216–224.
7. Christensen KA, Grant DM, Schulman EM, Walling C. Optimal determination of relaxation times of Fourier transform nuclear magnetic resonance. Determination of spin-lattice relaxation times in chemically polarized species. *J Phys Chem*. 1974;78(19):1971–1977.
8. Gupta RK. A new look at the method of variable nutation angle for the measurement of spin-lattice relaxation times using Fourier transform NMR. *J Magn Reson*. 1977;25(1):231–235.
9. Homer J, Beevers MS. Driven-equilibrium single-pulse observation of $T_1$ relaxation. A reevaluation of a rapid "new" method for determining NMR spin-lattice relaxation times. *J Magn Reson*. 1985;63(2):287–297.
10. Look DC, Locker DR. Time saving in measurement of NMR and EPR relaxation times. *Rev Sci Instrum*. 1970;41(2):250–251.
11. Markl M, Leupold J. Gradient echo imaging. *J Magnet Reson Imaging*. 2012;35(6):1274–1289.
12. Shulman RG, Rothman DL. $^{13}C$ NMR of intermediary metabolism: implications for systemic physiology. *Annu Rev Physiol*. 2001;63(1):15–48.
13. Maher EA, Marin-Valencia I, Bachoo RM, et al. Metabolism of [U-$^{13}C$]glucose in human brain tumors in vivo. *NMR Biomed*. 2012;25(11):1234–1244.
14. van Zijl PC, Rothman D. NMR studies of brain $^{13}C$-glucose uptake and metabolism: present status. *Magn Reson Imaging*. 1995;13(8):1213–1221.
15. Ross B, Lin A, Harris K, Bhattacharya P, Schweinsburg B. Clinical experience with $^{13}C$ MRS in vivo. *NMR Biomed*. 2003;16(6–7):358–369.
16. de Graaf RA, Mason GF, Patel AB, Behar KL, Rothman DL. In vivo $^{1}H$-[$^{13}C$]-NMR spectroscopy of cerebral metabolism. *NMR Biomed*. 2003;16(6–7):339–357.
17. Sonnewald U, Kondziella D. Neuronal glial interaction in different neurological diseases studied by ex vivo $^{13}C$ NMR spectroscopy. *NMR Biomed*. 2003;16(6–7):424–429.
18. Magnusson I, Rothman DL, Jucker B, Cline GW, Shulman RG, Shulman GI. Liver glycogen turnover in fed and fasted humans. *Am J Physiol*. 1994;266(5 pt 1):E796–E803.
19. Perseghin G, Petersen K, Shulman GI. Cellular mechanism of insulin resistance: potential links with inflammation. *Int J Obes Relat Metab Disord*. 2003;27(suppl 3):S6–S11.
20. Boesch C. Musculoskeletal spectroscopy. *J Magn Reson Imaging*. 2007;25(2):321–338.
21. Werner I, Bacher A, Eisenreich W. Retrobiosynthetic NMR studies with $^{13}C$-labeled glucose. *Formation of gallic acid in plants and fungi*. *J Biol Chem*. 1997;272(41):25474–25482.
22. Allouche-Arnon H, Wade T, Waldner LF, et al. In vivo magnetic resonance imaging of glucose—initial experience. *Contrast Media Mol I*. 2013;8(1):72–82.
23. Rodrigues TB, Serrao EM, Kennedy BW, Hu DE, Kettunen MI, Brindle KM. Magnetic resonance imaging of tumor glycolysis using hyperpolarized $^{13}C$-labeled glucose. *Nat Med*. 2014;20(1):93–97.
24. Meier S, Karlsson M, Jensen PR, Lerche MH, Duus JO. Metabolic pathway visualization in living yeast by DNP-NMR. *Mol Biosyst*. 2011;7(10):2834–2836.
25. Miclet E, Abergel D, Bornet A, Milani J, Jannin S, Bodenhausen G. Toward quantitative measurements of enzyme kinetics by dissolution dynamic nuclear polarization. *J Phys Chem Lett*. 2014;5(19):3290–3295.

26. Ferretti A, Bozzi A, Di Vito M, Podo F, Strom R. $^{13}C$ and $^{31}P$ NMR studies of glucose and 2-deoxyglucose metabolism in normal and enzyme-deficient human erythrocytes. *Clin Chim Acta*. 1992;208(1–2):39–61.
27. Kotyk JJ, Rust RS, Ackerman JJH, Deuel RK. Simultaneous in vivo monitoring of cerebral deoxyglucose and deoxyglucos-6-phosphate by $^{13}C\{^1H\}$ nuclear magnetic resonance spectroscopy. *J Neurochem*. 1989;53(5):1620–1628.
28. Nasrallah FA, Pages G, Kuchel PW, Golay X, Chuang KH. Imaging brain deoxyglucose uptake and metabolism by glucoCEST MRI. *J Cereb Blood Flow Metab*. 2013;33(8):1270–1278.
29. Sokoloff L, Reivich M, Kennedy C, et al. The [$^{14}C$]deoxyglucose method for the measurement of local cerebral glucose utilization: theory, procedure, and normal values in the conscious and anesthetized albino rat. *J Neurochem*. 1977;28(5):897–916.
30. Bossenne V, Firmin P, Perly B, Berthault P. Use of selective excitation techniques for the rapid analysis of $^{13}C$ NMR data for enriched carbohydrates. *Magn Reson Chem*. 1990;28(2):149–155.
31. Cohen DM, Wei J, O'Brian Smith E, Gao X, Quast MJ, Sokoloff L. A method for measuring cerebral glucose metabolism in vivo by $^{13}C$-NMR spectroscopy. *Magn Reson Med*. 2002;48(6):1063–1067.
32. Roslund MU, Tahtinen P, Niemitz M, Sjoholm R. Complete assignments of the (1)H and (13)C chemical shifts and J(H,H) coupling constants in NMR spectra of D-glucopyranose and all D-glucopyranosyl-D-glucopyranosides. *Carbohydr Res*. 2008;343(1):101–112.
33. Walker TE, London RE, Whaley TW, Barker R, Matwiyoff NA. Carbon-13 nuclear magnetic resonance spectroscopy of [1-$^{13}C$] enriched monosaccharides. Signal assignments and orientational dependence of geminal and vicinal carbon-carbon and carbon-hydrogen spin-spin coupling constants. *J Am Chem Soc*. 1976;98(19):5807–5813.
34. Herve M, Wietzerbin J, Tran-Dinh S. Non-cooperative effects of glucose and 2-deoxyglucose on their metabolism in *Saccharomyces cerevisiae* studied by $^1H$-NMR and $^{13}C$-NMR spectroscopy. *Eur J Biochem*. 1993;218(1):221–228.
35. Navon G, Lyon RC, Kaplan O, Cohen JS. Monitoring the transport and phosphorylation of 2-deoxy-D-glucose in tumor cells in vivo and in vitro by $^{13}C$ nuclear magnetic resonance spectroscopy. *FEBS Lett*. 1989;247(1):86–90.
36. Chang LC, Koay CG, Basser PJ, Pierpaoli C. Linear least-squares method for unbiased estimation of $T_1$ from SPGR signals. *Magn Reson Med*. 2008;60(2):496–501.